

Development of a silicon drift detector array; An x-ray fluorescence spectrometer for remote surface mapping

Jessica A. Gaskin^{*a}, Gabriella A. Carini^b, Wei Chen^b, Ronald F. Elsner^a, Georgiana Kramer^c,
Gianluigi De Geronimo^b, Jeffrey W. Keister^b, Zheng Li^b, Brian D. Ramsey^a, Pavel Rehak^b,
D. Peter Siddons^b

^aSpace Science Office, VP62, NASA Marshall Space Flight Center, Huntsville, AL 35812, USA;

^bBrookhaven National Laboratory, Upton, NY 11973, USA

^cBear Fight Center, Winthrop, WA 98862

ABSTRACT

Over the past three years NASA Marshall Space Flight Center has been collaborating with Brookhaven National Laboratory to develop a modular Silicon Drift Detector (SDD) X-Ray Spectrometer (XRS) intended for fine surface mapping of the light elements of the moon. The value of fluorescence spectrometry for surface element mapping is underlined by the fact that the technique has recently been employed by three lunar orbiter missions; Kaguya, Chandrayaan-1, and Chang'e. The SDD-XRS instrument we have been developing can operate at a low energy threshold (i.e. is capable of detecting Carbon), comparable energy resolution to Kaguya (<150 eV at 5.9 keV) and an order of magnitude lower power requirement, making much higher sensitivities possible. Furthermore, the intrinsic radiation resistance of the SDD makes it useful even in radiation-harsh environments such as that of Jupiter and its surrounding moons.

Keywords: Silicon Drift Detector, x-ray spectrometer, lunar elemental mapping, Jupiter elemental mapping, x-ray optics

1. INTRODUCTION

NASA has recently set its sights on achieving two major goals: the return of humans to the moon¹ and the launch of an Outer Planet Flagship Mission to the Jovian system² both by 2020. In both instances, improved instrumentation (e.g. enhanced sensitivity, low power, etc...) is desired. To this end, NASA Marshall Space Flight Center (MSFC) and Brookhaven National Laboratory (BNL) have been collaborating to develop a novel modular Silicon Drift Detector (SDD) X-Ray Spectrometer (XRS) for measuring the abundances of light surface elements (C to Fe) fluoresced by ambient radiation. Two versions of this XRS are currently under development; the first has a large sensitive area and is suitable for orbit around the moon and the second is a more radiation-resistant, high-speed version for use in a radiation hard environment such as that of Jupiter and Europa. The accurate measurement of major elemental concentrations using the modular Silicon Drift Detector - X-Ray Spectrometer (SDD-XRS) described here, will enhance our existing scientific knowledge of the two systems and better prepare us for a lasting human presence on the moon.

Recently, there have been three major lunar orbiter missions that have made use of an XRS. Of these three, the XRS instrument aboard the Japanese SELENE/Kaguya mission (which impacted the lunar surface June 10, 2009) was the most sensitive with 100 cm² of collecting area, and <180 eV resolution at 5.9 keV³. The SDD-XRS instrument that we have been developing offers comparable energy resolution⁴, lower energy threshold^{5,6} and an order of magnitude lower power requirement⁷, making much higher sensitivities possible with modest spacecraft resources. In addition, even in its unhardened form, the SDD-XRS is significantly more radiation resistant than x-ray CCDs and therefore will not be subject to the degradation seen by previous lunar XRS instruments³. To date, the majority of the SDD-XRS development has been on prototyping a lunar version of the SDD-XRS. As such, this version is the focus of this paper.

* Jessica.Gaskin@nasa.gov; phone 1 256 961-7818; fax 1 256 961-7522

However, the SDD-XRS is flexible in that it permits scaling to much larger areas. In this large format, the SDD array can be used for elemental mapping of other solar system objects in addition to the Moon, such as Mercury, near-earth asteroids, the Martian satellites, and comets. In these applications the ambient charged-particle background rate is low, the surface fluorescence being stimulated by solar radiation. Thus, large-area, simply-collimated detectors are sufficient for these applications. The advantage of the SDD detector array is that these large areas can be achieved with very modest power consumption, typically an order of magnitude less than competing CCDs.

Further, the intrinsic radiation resistance of the SDD makes it applicable to the harsh environment of the Jovian system where it can be used to map the light surface elements of Europa. Located in an intense radiation field, this moon is bombarded with a large flux of electrons and ions which give rise to x-ray fluorescence characteristic of the surface elements. A modified version of the lunar SDD-XRS combined with a nested array of grazing incidence x-ray optics, would allow one to distinguish these lines against a large background continuum, to give a unique measure of Europa's surface composition while in orbit around it. The use of optics is dictated by the harsh radiation environment which would swamp a large-area instrument. Focusing source flux onto a small detector significantly enhances signal to noise ratio, reduces the overall telemetry requirement, and facilitates shielding. Our group has recently started design and fabrication of a Jupiter-Europa SDD-XRS, which will require the development of high-speed read-out electronics that will be matched to appropriate SDDs (similar to those used for the lunar SDD-XRS).

2. LUNAR ORBITING X-RAY SPECTROMETER

2.1 Lunar Science

The value of global element mapping is evident from the number of past, present and future lunar missions that feature this capability. The Apollo 15 and Apollo 16 x-ray spectrometers covered a small area (~9%) of the nearside equatorial regions of the Moon with a spatial resolution of ~100 km and energy resolution of ~800 eV at 6.4 keV, and reported Al/Si and Mg/Si ratios⁸. Clementine provided high resolution (~250 m/pixel) global estimates of the concentrations of FeO and TiO₂ based on algorithms applied to multi-spectral reflectance data⁹. These data have a systematic error, however, demonstrated by comparing the spectrometer data of all landing sites with their respective samples^{10,11,12} and by comparison with elemental abundances measured by Lunar Prospector's Gamma-Ray Spectrometer^{13,14}.

The science goals of these three instruments can be found in detail in several recent publications^{Error! Bookmark not defined.,15,16,17}. The science goals of the SDD-XRS overlap those laid out by Kaguya-XRS and Chandrayaan-1 C1XS, to ultimately - trace the geological and thermal evolution of the Moon.

- *Measure global abundances. Given the concentrations of the six most abundant elements after O (i.e. Si, Al, Ti, Fe, Mg, and Ca) it is possible to calculate the relative proportions of the four major minerals that uniquely account for major mineral concentrations, namely plagioclase, pyroxene, olivine, and ilmenite. This "normative mineralogy" provides information to identify the likely rock types of which the regolith is composed. The ability to measure concentration values as low as 1% are highly desirable for this study.*
- *Map crater basins and identify materials that originate from the deep lunar interior by observing crater central peaks and impact ejecta.*
- *Determine the magnesium number (Mg') of the lower crust and mantle. The leading theory of the formation of the Moon begins with a Mars-sized object impacting the proto-Earth at 4.6Ga^{18,19,20}. Based on this theory and the techniques of forensic petrology, elemental abundances of the lunar surface can yield insight into the Moon's formation and evolution.*
- *Measure the major element geochemistry in the main lunar terrain types (i.e. Procellarum KREEP [Potassium, Rare Earth Elements, and Phosphorous] Terrain, South Pole-Aitken Basin, and the Far-side Highlands). KREEP basalts, for example, have an anomalously-high Mg' and are associated with the last remains of the Lunar Magma Ocean (LMO)^{21,22}. Knowing the spatial distribution of the Mg' at higher resolution would provide insight into the lunar crust's formation.*

- *Verify assertions that the Moon is heavily depleted in volatiles, iron and iron-associated elements, and enriched with refractory elements - such as Al^{23,24,25,26}. Higher-spatial-resolution Mg and Al maps will allow for direct detection of unique lithologies, like high-Al mare basalt units within a mare-filled basin, that are currently only possible through indirect means^{27,28}. At a fine resolution, discrete lava flows can be mapped that distinguish the Mg/Al, Mg/Si, and Al/Si ratios, which can aid in delineating mare basalt unit boundaries (e.g., Mare Crisium²⁹).*

Higher-sensitivity measurements than those currently planned or carried out to date would permit a significant enhancement of many of the science goals stated above (such as crater and lava flow mapping which are relevant on much finer scales). Further, the SDD-XRS, would address additional goals such as the identification of potential landing sites for future unmanned and manned missions, based on resource utilization and geologically interesting formations.

The intrinsic radiation resistance of a high-resolution XRS would return abundance maps of significantly smaller impact craters than currently available, providing more surface details and shallow subsurface information, based on the simple crater depth : diameter ratio³⁰ \approx 1:10. Lunar craters with diameters larger than ~15 km typically exhibit more complex morphologies³¹. Larger craters and basins will benefit from a high-spatial-resolution elemental mapper to distinguish chemical differences associated with fine interior structures (e.g. rim, walls, floor, central peak, ejecta, and secondary impacts). Likewise, the diameters of central crater peaks are generally less than tens of km across. These central peaks consist of material from deep within the crater (and possibly the mantle), so knowledge of their composition is key to understanding the geology of the local region, the underlying (mantle) composition, and the region's context in the geological evolution of the whole Moon. The ~20-km-diameter crater Copernicus offers an excellent example. Multispectral evidence indicates the central peak of Copernicus has an anomalously high abundance of olivine^{32,33,34,35}, suggesting that the impact may have tapped the lunar mantle.

The addition of compositional data can significantly improve upon age estimation of the lunar surface using crater-size frequency distributions^{36,37} or more complex techniques involving secondary craters, craters within other craters and basins, and crater degradation,^{38,39}. The ability to directly link relative ages with discrete surface compositions enables the geologist to deduce lunar mantle processes over time and in three-dimensional space. Since the Moon acts as a lodestar for planetary evolution and recorder of solar system history, knowledge gained from these studies can be applied to planets including the Earth^{40,41,42,43,37,44}.

2.2 Lunar landing site identification & resource utilization

One of the main objectives of the NASA Lunar Program is to carry out landing site identification and certification on the basis of potential resources. The ability to clearly identify the four major lunar minerals; ilmenite, anorthite, pyroxene, and olivine and distinguish some mineral series endmembers (e.g., clinopyroxene vs. orthopyroxene), through their elemental abundance ratios, is key to their mapping. Of the four major minerals, ilmenite and anorthite are excellent sources for oxygen extraction^{45,46}. Therefore, maps of their distributions are in high demand for in-situ resource identification and utilization. Other important and identifiable resources include silicates, lunar glasses (rich in iron), or lunar regolith from the Maria or highlands.

2.3 Lunar instrument concept

Sensitive mapping of the surface elements of the moon necessitates a spectrometer with very good energy resolution. This ensures that closely spaced fluorescent lines are well separated and also that the lines can be resolved above the underlying (background) continuum of scattered radiation from the lunar surface. In addition, the spectrometer must have as large an area as possible within available resources to give the greatest sensitivity for element detection and/or the smallest resolution on the ground. We derive a set of preliminary instrument requirements, listed in Table 1, to give the desired sub-10-km resolution and 1% abundance sensitivity for the principal lunar surface elements, assuming modest spacecraft resources.

Table 1. Lunar elemental mapper detector requirements

Total Area	$\sim 500 \text{ cm}^2$
Energy Range	$< 0.2 - 7 \text{ keV}$
Energy Resolution	$\leq 100 \text{ eV FWHM @ } 0.28 \text{ keV}$
Radiation Hardness	$> 10 \text{ krad}$
Power (including processing)	$\sim 10 \text{ Watts}$
Field of View (collimated)	$10 \text{ deg} \times 10 \text{ deg}$

We have simulated the expected performance using this simply-collimated-detector specification and show this in **Error! Reference source not found.**, using global estimates of the element abundances, and an 8.7 km x 8.7 km surface footprint. For this estimation we have used a 50 km altitude orbit and a 1-year mission time, which gives an effective (minimum) integration time at the equator of 22 sec per image element. The solar x-ray flux was taken as an average expected around solar maximum.

The fluorescent lines of oxygen (K), iron (L), sodium (K), magnesium (K), aluminum (K), silicon (K) and calcium (K) are clearly resolved with this spatial resolution for input abundances of 44%, 6%, 1%, 5%, 13%, 21% and 10% respectively. We estimate from these preliminary simulations that this configuration could achieve better than 1% abundance sensitivity with 8.7 km resolution for all the elements listed above.

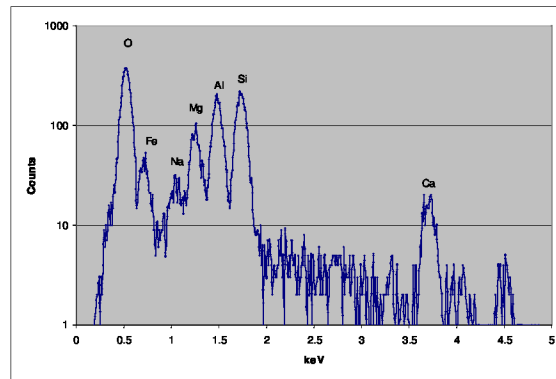


Fig. 1. Simulated response of the strawman payload with 8.7 km footprint

3. SDD-XRS DEVELOPMENT

3.1 Detector overview

Over the past three years MSFC and BNL have developed a prototype lunar XRS (which will be adapted to meet requirements for a Europa mission). The primary achievements of this instrument are superior energy resolution, low power (substantially less power than that used by CCDs) and significant radiation hardness negating any concerns regarding possible radiation damage.

The SDD, first conceived by Gatti and Rehak⁴⁷, is a device fabricated from fully depleted silicon in which a series of shaping electrodes define a drift path for photoionization electrons to a small collection anode. In the configuration relevant to this development, the electric field, generated by a spiraling resistive drift electrode (biased only at its inner and outer point) on the top side of a wafer, forces the signal electrons, generated by the absorption of an incident x ray, to a small sized anode in the center of the device^{48,49}. There is no region of low field so all electrons in the sensitive area are guided within 100 ns to the readout node. Fig. 2 shows the electrode configuration for a single hexagonal SDD pixel, the shape used for our application. The entrance window is on the hidden (lower) face of the pixel^{5,6}. This window acts as a continuous thin rectifying junction through which the x-rays enter the detector. The side of the detector opposite the window is called the device side. This side contains the electron central collecting anode, spiral drift electrodes, and sink anode necessary to generate the drift field and to sink any leakage current.

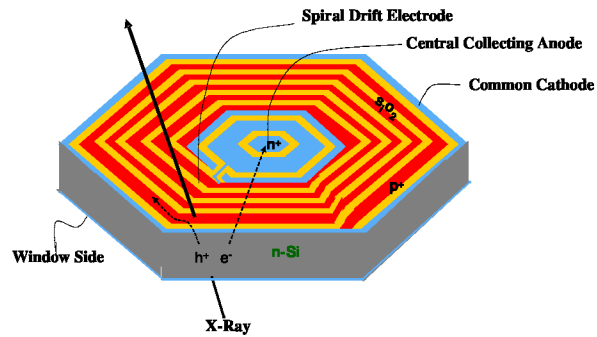


Fig. 2. Schematic of a hexagonal silicon drift detector pixel

A distinct advantage of the SDD is that the capacitance of the tiny collection anode is less than 0.1 pF and independent of the size of the detector. This small capacitance makes it possible to design read-out electronics with very low noise, even with a bonded connection between the anode and the integrated preamplifier⁵⁰. This ensures excellent energy resolution even with relatively large pixels (by CCD standards).

Typical SDDs are a few mm across, but the devices can be arrayed, with a common outer (drift-biasing) cathode, on a single wafer of silicon. When combined with custom readout electronics, a modular design can be arrived at, permitting large areas to be covered with very low power requirements (an order of magnitude less than typical x-ray CCDs), and modest cooling requirements (typically -30 °C). In addition, the devices are very radiation tolerant. This combination of characteristics makes the SDD ideally suited for orbiting XRSs around a variety of planetary objects in our solar system.

3.2 Lunar SDD-XRS prototype

The lunar SDD-XRS will primarily consist of a large array of SDDs (~500cm²) coupled to custom low-noise readout electronics and a simple mechanical collimator which will be used to define the field of view on the lunar surface. The main function of these detectors are to read out the energy of individual x-rays for elemental composition determination (<0.2-7keV) and their associated time of detection, which will give their origination position on the surface.

The first MSFC-BNL lunar SDD-XRS prototype was made up of an array of 14 SDD pixels (plus 2 additional test pixels), each ~ 5 mm in diameter, coupled to an ASIC with 14 channels. Initial instrument design work was completed at BNL and test detectors were fabricated, both at BNL (Semiconductor Detector Development and Processing Lab in the Instrumentation Division) and at KETEK GmbH, along with the custom Application Specific Integrated Circuits (ASICs) that read out these detector arrays. Limiting the ASIC to just 14 individual detectors meant that bond lengths linking the detector to the ASIC readout electronics could be short which ensures low readout noise and good energy resolution. A 14-detector unit cell is shown in Figure 3. Two different detector patterns are present, one of which has a spoke pattern (field plate) for additional field definition^{5,6}.

Many different electrode configurations were simulated at Brookhaven National Laboratory for the silicon drift detector and 24 different patterns were fabricated for testing, each based on the same-sized SDD, but with subtly different electrode configurations. In parallel with this effort, the custom readout chip was simulated, designed, fabricated (through the MOSIS prototyping and small-volume chip production service) and tested⁷.

The current MSFC-BNL lunar SDD-XRS is made up of 64 spiral SDDs, fabricated on a 4" wafer, by KETEK GmbH and is shown in Figure 4. The choice of electrode configuration for these SDDs was based on test results from the previous prototype. Once again, each SDD acts as an individual pixel cell and each array is matched to an Application Specific Integrated Circuit (ASIC) – front-end electronics that contain the control and readout logic, multiplexers, common bias circuitry, registers, DACs, and temperature sensor⁴. These second generation ASICs have 16 channels, rather than 14 channels, requiring 4 be tiled together to match the full number of pixel cells. Each pixel cell is a hexagonal SDD that contains a low capacitance anode at its center, towards which the generated electron signal will drift. These central anodes are wire-bonded directly to a corresponding ASIC input. The ASIC and PC board interface have been redesigned to minimize bond lengths. Reducing the length of the wire bonds between the ASIC and SDD pixel cells reduces pick-up, which may lead to noise in the system. This 64 pixel SDD array & ASIC combination can

be tiled with additional units, such that the desired collecting area is achieved which will be based on mission requirements (i.e. time in orbit around the moon, orbit altitude and power constraints).

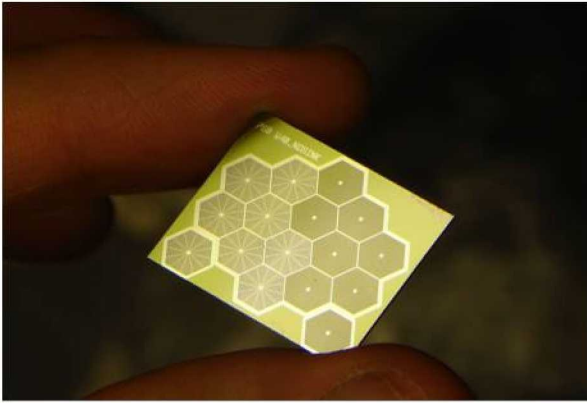


Fig. 3. A 14-SDD array fabricated on a silicon wafer (with two additional test pixels)

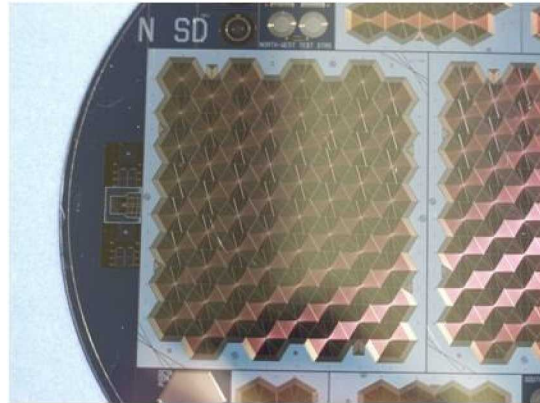


Fig. 4. The figure shows an image of a single 64-pixel cell SDD array. Each hexagonal pixel has an active area of 20 mm².

4. TESTING & RESULTS

This section summarizes some of the testing and key results for both SDD-XRS prototypes described above. Further details and more in-depth discussion on the detector fabrication, design and testing, and ASIC design and testing can be found in references [4], [5], [6], and [7] co-author publications.

4.1 SDD-XRS prototype: 14-pixel Array

Initial electrical characterization of the test arrays permitted down selection of several of the most promising patterns for x-ray testing at the National Synchrotron Light Source (NSLS) located at BNL. These detectors were wire bonded to the ASICs and initial bench-top x-ray tests were carried out in a dedicated vacuum system with a flood illumination source (⁵⁵Fe at 5.9 and 6.4 keV) shining through a beryllium window for overall performance assessment. The best energy resolution for a single pixel was measured to be 146 eV at 5.9 keV (obtained at -35°C), and is approaching the project energy resolution goal of 140 eV necessary to resolve low-energy fluorescent lines. However, there were pixels that exhibited worse energy resolution, some at 170 eV at 5.9 keV, most likely due to the various wire bond lengths between the ASIC and SDD pixel elements and to our cooling scheme. The operating power of the detector array with its custom electronics was measured to be < 2 mW/channel, or about 10 mW/cm²; an order of magnitude lower than typical CCDs.

These initial screening tests were followed by detailed beamline tests at the NSLS. Figure 5 shows a test silicon drift detector (SDD) array mounted on a cold finger for insertion into the UV beamline U3C. The electronic readout PC board is visible with the ASIC at its center. The SDD array is mounted directly underneath this and is not visible.

Beamline tests at the synchrotron enabled fine probing (25-micron-diameter beam) of the arrays at a range of precisely-defined energies. Figure 6 shows the response measured at 900 eV (taken at -27°C). The energy resolution was found to be 139eV and 161eV for a single pixel on a BNL and KETEK detector, respectively. The difference in the response is due to the fact that the detectors have slightly different electrode patterns and as such, they were biased using somewhat different voltages. Also, the KETEK pixel under study had a longer wire bond length than that of the BNL pixel element. Because the two detectors were fabricated at two different locations, the resistivity of the material is also slightly different for the two detectors. The BNL detector array is n<111>, is 350μm thick and resistivity of >4k Ωcm. The KETEK is n<100>, and is 400 μm thick with resistivity of 7.5k Ωcm.

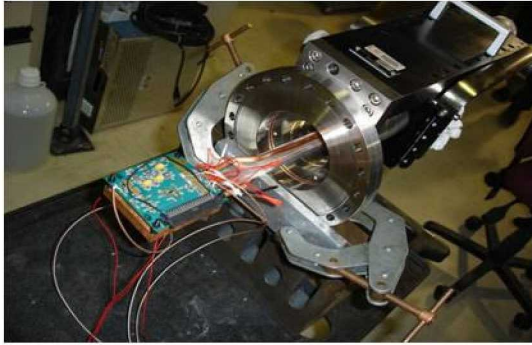


Fig. 5. Image of the SDD-XRS installed in the UV beamline U3C at the NSLS. The ASIC and PC board interface are visible.

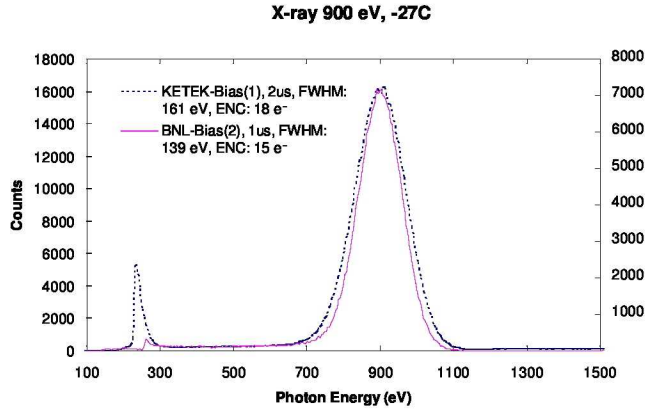


Fig. 6. Histogram of 900eV X-Rays for single pixels on a BNL and KETEK SDD array.

In addition, a two-stage X-Y actuator system was used to scan this 25 μm beam, with 600 μm steps in the X-direction and 700 μm steps in the Y-direction, across the length of a pixel element on one of the KETEK detector arrays to determine the uniformity of the response. Measurements were taken with beam energy of 900eV and at -27°C. Figure 7a shows a diagram of the single pixel scan path and Figure 7b shows the resulting response as a function of scan position for two slightly different bias conditions. The measured response is fairly uniform across the pixel, however, it is clear that the choice of bias impacts detector performance.

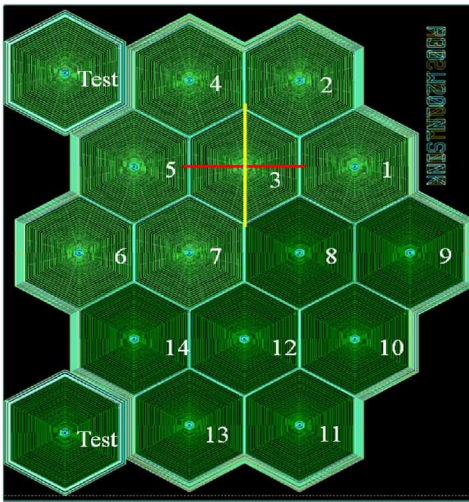


Fig. 7a. Image of the 14-pixel SDD-XRS (plus 2 test pixels). The yellow line denotes the vertical scan and the red line denotes the horizontal scan of the 25 μm x-ray beam.

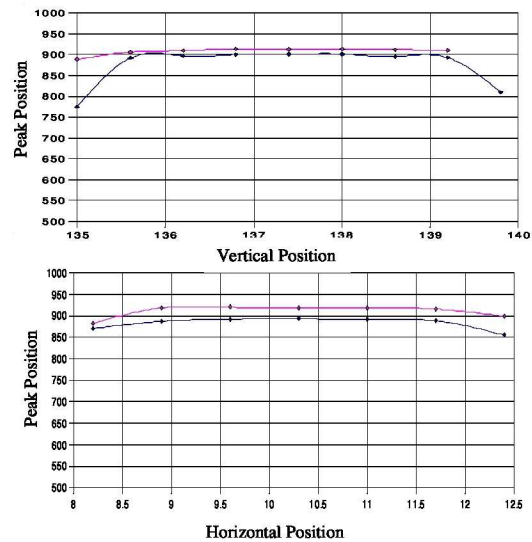


Fig. 7b. Plot of the response across the pixel in the vertical and horizontal directions for two different bias conditions on the same detector.

The ability to measure carbon fluorescence at 0.28 keV is highly desirable as this maximizes the potential applications for this device. This goal necessitates not only slightly lower noise but also a very thin entrance window. Based on models of the lunar surface visible brightness, we calculated that a 110 nm layer of aluminum is necessary on the entrance to the SDDs to reduce leakage current from ambient light to below the quiescent value for the cooled detector. This aluminum layer, plus an oxide layer on the silicon, constitutes a minimum amount of material on the input to the SDD and defines the low-energy-photon cut-off energy. To assess this low-energy response, we measured the absolute efficiency of the detectors, coated with the requisite 110 nm of aluminum, as a function of energy in the critical region below 1 keV. These data are shown in Figure 8.

Two sets of data are presented in Figure 9, one set for a Brookhaven-fabricated device and one for a device from the commercial vendor (KETEK). It can be seen that the KETEK device had higher throughput at lower energies and gave a best fit oxide-layer thickness, significantly less than the BNL device. In other respects, such as uniformity and energy resolution, the BNL and KETEK devices gave similar performance. The efficiencies were measured in two different ways, a current mode and a counting mode, for each device. Both methods gave similar results.

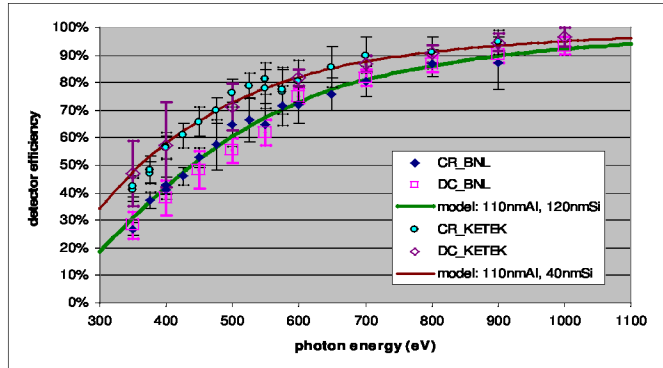


Fig. 8. Absolute efficiency of two test detectors as a function of energy

These tests show that the detector + custom electronics are operating close to their performance goal, limited by some additional noise in the readout electronics. This noise includes both ASIC-generated component and a capacitance component that arises due to the pad layout on the detectors. As mentioned earlier, a new version of the ASIC has been designed and fabricated. The new ASIC design addresses all relevant issues affecting the previous version, including peak detector stability, limited dynamic range, and charge amplifier parasitics, and features lower power dissipation, higher resolution, higher charge gain, on-board temperature sensors, and a fully differential analog and digital interface. This new ASIC + detector combination should reduce the total noise component from its current 16 electrons RMS (170 eV FWHM at 5.9 keV) to just 11 electrons RMS. This in turn should bring the energy resolution down to our goal of 140 eV at 5.9 keV and just 90 eV at the carbon K line of 0.28 keV.

4.2 SDD-XRS prototype: 64 pixel array

The 64 pixel SDD-XRS has been benchtop tested at BNL under flood illumination with a ^{55}Fe source. Figure 9 shows the resulting spectrum in which several lines are easily distinguished. In addition to the silicon $\text{K}\alpha$ and $\text{K}\beta$ escape peaks, Mn, Ti, Ar, and Ca are also visible (generated via fluorescence of the surrounding structure induced by the ^{55}Fe source).

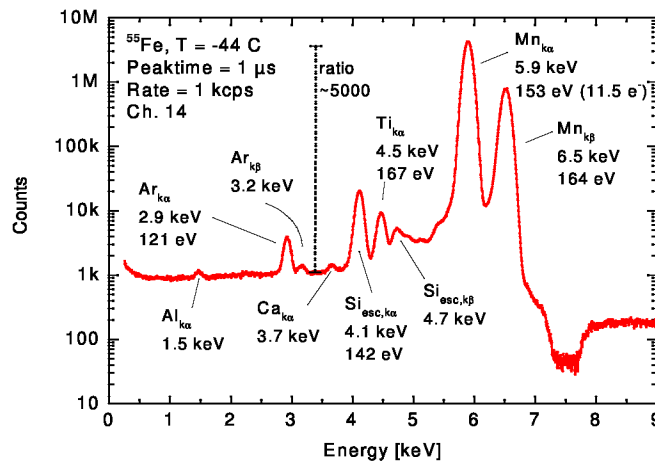


Fig. 9. Spectrum taken of a single pixel on the 64 element SDD array. The peak to valley ratio for the Mn $\text{K}\alpha$ line is $\sim 5000^4$.

We hope to improve on this energy resolution by optimizing the bias conditions (i.e. using a slightly larger negative voltage to the electrode surrounding the anode to further decrease the anode capacitance)⁴. We also expect an improved detector response once the new ASIC (read-out electronics) is employed.

5. CONCLUSIONS

The primary goal of this effort is to develop a new type of x-ray detector to be used in Lunar remote sensing, that would have excellent energy resolution and low-energy threshold (for observing the carbon K α line), use substantially less power than the CCDs, and that would have significant radiation hardness negating any concerns regarding possible radiation damage. Results from our preliminary testing indicate that we are on track to realizing this ambition.

Short-term plans are to fully characterize the 64 pixel SDD-XRS array at the NSLS in the UV beamline U3C this Fall (August 2009) and again when the new test-cycle starts later in the year. Final testing will be done using the SDD pixel array described here, the redesigned ASIC and interface board. In parallel we plan on completing a preliminary thermal study, to ensure that passive cooling alone will be adequate, and on completing a lunar radiation model for sensitivity assessment.

Once we have achieved our goals for the lunar SDD-XRS, we plan on developing a Jupiter-Europa version of the SDD-XRS which will involve the fabrication of thin n-type devices with increased doping levels. These will be tested, first at BNL to assess their overall performance and then at the University of Indiana Cyclotron Facility to gauge their radiation hardness. While performing radiation tests of the detectors, we shall also irradiate our existing Lunar ASICs to provide useful data for the design of the high-speed, radiation-resistant versions. In parallel with this, we shall begin the design, fabrication and testing of sub-circuits, primarily for high-speed operation of a new ASIC, necessary for SDD-XRS operation in the Jovian environment. Fabrication and testing of these new detectors + high-speed ASIC will commence. The complete detector assemblies will be characterized and will include measurements of quantum efficiency and resolution, as a function of energy, and rate capability. During this period we will also subject several completed detector + ASIC units to various radiation doses to confirm their hardness.

ACKNOWLEDGEMENTS

This work is mainly funded through the NASA Research Opportunities in Space and Earth Sciences, Planetary Instrument Definition and Development Program NNH08ZDA001N-PIDD. We would like to thank Brookhaven National Laboratory (BNL) and the New Jersey Institute of Technology for their cost-sharing in the development of the high-speed radiation-hard electronics portion of this effort. We would also like to acknowledge the support of additional BNL team members who have supplied technical support throughout this project (J. Fried, D. Pinelli, J. Triolo, E. Vernon, and T. Lenhard).

REFERENCES

-
- ^[1] Bush, G. W., "A Renewed Spirit of Discovery: The President's Vision for U.S. Space Exploration," NASA Technical Document, NP-2004-01-334-HQ (2004).
 - ^[2] Clark, K., Magner, T., Pappalardo, R., Blanc, M., Greeley, R., Lebreton, J. P., Jones, C., Sommerer, J., "Jupiter Europa Orbiter Mission Study 2008: Final Report," The NASA Element of the Europa Jupiter System Mission Technical Document, Task Order #NMO710851 (2009).
 - ^[3] Okada, T., Shiraishi, H., Shirai, K., Yamamoto, Y., Arai, T., Ogawa, K., Kato, M., Grande, M., and the SELENE XRS Team, "X-Ray Fluorescence Spectrometer (XRS) On Kaguya: Current Status and Results," 40th LPSC (2009).
 - ^[4] Rehak, P., Carini, G., Chen, W., De Geronimo, G., Fried, J., Li, Z., Pinelli, D., Siddons, D. P., Vernon, E., Gaskin, J. A., Ramsey, B., "Arrays of Silicon Drift Detectors For an Extraterrestrial X-Ray Spectrometer," NIM A (2009).

-
- [5] Chen, W., Carini, G., De Geronimo, G., Fried, J., Gaskin, J. A., Keister, J. W., Li, Z., Ramsey, B. D., Rehak, P. and Siddons, D. P., "Development of Thin-Window Silicon Drift Detector for X-Ray Spectroscopy," IEEE Nuclear Science Symposium Conference Record, N33-4 (2007).
- [6] Carini, G. A., Chen, W., De Geronimo, G., Gaskin, J. A., Keister, J. W., Li, Z., Ramsey, B. D., Rehak, P. and Siddons, D. P., "Performance of Thin-Window Silicon Drift Detectors", IEEE Nuclear Science Symposium Conference Record, N28-2 (2008).
- [7] De Geronimo, G., Chen, W., Fried, J., Rehak, P., Vernon, E., Gaskin, J. A., and Ramsey, B. D., "Front-End ASIC for High Resolution X-Ray Spectrometers," IEEE Nuclear Science Symposium Conference Record, N03-5 (2007).
- [8] Adler, I., et al. 1973, *The Moon*, 7, 487-504
- [9] Lucey, P. G., Blewett, D. T., & Hawke, B. R. 2000, *J. Geophys. Res.* 105 (E8), 20377-20386
- [10] Blewett, D. T., Lucey, P. G., Hawke, B. R., & Jolliff, B. L. 1997, *J. Geophys. Res.* 102 (7), 16319-16325
- [11] Giguere, T. A., Taylor, G. J., Hawke, B. R., & Lucey P. G. Jan. 2000, *Meteoritics & Planetary Sci.* 35, 193-200
- [12] Korotev, R. L., & Gillis, J. J. 2001, *J. Geophys. Res.* 106, 12339-12354
- [13] Prettyman, T. H., et al. 2002, LPSC XXXIII, No 2012
- [14] Shkuratov, Y., et al. 2004, LPSC XXXIII, 1162
- [15] Barbera, M. et al., 2007, Proc. SPIE 6686, 668615-1 to 668615-13
- [16] Grande, M. et al., 2008, LPSC XXXIX, No 1391, 1620
- [17] Joy, K., et al. 2008, LPSC XXXIX, No 1391, 1070
- [18] Hartmann, W. K., & Davis D. R. 1975, *Icarus* 24, 504-515
- [19] Cameron, A. G. W., & Ward, W. R. 1976, Abstracts of LPSC 7, 120
- [20] Wood, J. A. 1986, *Origin of the Moon*, eds. W. K. Hartmann, R. J. Phillips, & G. J. Taylor (Lunar Planet. Inst., Houston, TX), 17-55
- [21] Warren, P. H., & Wasson, J. T. 1979b, *Rev. Geophys. Space Phys.* 17, 73-88
- [22] Shearer, C. K., & Papike, J. J. 1999, *Amer. Mineral.*, 84, 1469-1494
- [23] Taylor S. R. 1987, *Geochim. Cosmochim. Acta* 51, 1297-1309
- [24] Jolliff, B. L., Gillis, J. J., & Haskin, L. A. Mar. 2000, LPSC XXXI, No 1763
- [25] Elphic, R. C., et al. 2002, LPSC XXXIII, No 2009
- [26] Dunkin, S. K., et al. May 2003, *Planet. Space Sci.* 51, 435-442
- [27] Kramer, G. Y., Jolliff, B. L., & Neal, C. R. 2008a, *Icarus*
- [28] Kramer, G. Y., Neal, C. R., & Jolliff, B. L. 2008b, *J. Geophys. Res.* 113 (E1)
- [29] Andre, C. G., Wolfe, R. W., & Adler, I. 1978, In 'Mare Crisium: The view from Luna 24; Proceedings of the Conference', Houston, Tex., eds. R. B. Merrill and J. J. Papike (Pergamon Press, Inc., New York), 1-12
- [30] Melosh, H. J. 1989, *Impact Cratering: A Geologic Process* (Oxford University Press, New York, NY), 253
- [31] Pike, R. J. 1977, LPSC VIII, 3, 3427-3436
- [32] Pieters, C. M. Jan. 1982, *Science* 215, 59-61
- [33] Lucey, P. G., Taylor, G. J., Hawke, B. R., & Spudis P. D. 1998, *J. Geophys. Res.* 103 (E1), 1703-1713
- [34] Le Mouélic, S., Langevin, Y., & Erard, S. Mar. 2000, LPSC XXXI, No 1217
- [35] Cohen, J. L., & Pieters, C. M. Mar. 2001, LPSC XXXII, No 1034

-
- [36] Neukum, G., Konig, B., & Arkani-Hamed, J. 1975, *The Moon* 12, 201-229
- [37] Neukum, G. 1977, *Philosophical Transactions of the Royal Society of London* 285, 267-272
- [38] Boyce, J. M. 1976, *Proc. 7th Lunar Sci. Conf.*, 2717-2728
- [39] Boyce, J. M., & Johnson, D. A. 1978, *Proc. 9th Lunar Sci. Conf.*, 3275-3283
- [40] Goles, G. G., & Seymour, R. S. 1978, *Am. Geophys. Union* 59, 1214 (abstract)
- [41] Anderson, D. L. 2003, *Science* 213, 82-89
- [42] Nisbet, E. G., & Walker, D. 1982, *Earth Planet. Sci. Lett.* 60, 105-113
- [43] Hofmeister, A. M. 1983, *J. Geophys. Res.* 88, 4963-4983
- [44] Rubie, D. C., Melosh, H. J., Reida, J. E., C. L., & Richter K. 2003, *Earth Planet. Sci. Lett.* 205 (3-4), 239-255
- [45] Melendrez, D. E., Johnson, J. R., Larson, S. M., & Singer, R. B. Mar. 1994, *J. Geophys. Res.* 99, 5601
- [46] Rodriguez, R. Sep. 2000, In 'Exploration and Utilization of the Moon' (eds. B. H. Foing & M. Perry), 462 of ESA Special Publication. 251
- [47] Gatti, E. & Rehak, P. 1984, *Nucl. Instr. & Meth.* 225, 608
- [48] Lechner P., et al. 2001, *NIM A*, 458, 281
- [49] Struder, L. 2000, *Nucl. Instr. & Meth.* 454, 73
- [50] Gramegna, G., O'Connor, P., Rehak, P., & Hart, S. 1997, *IEEE Trans. Nucl. Sci.*, 44(3), 385